

Cycle Encoding of a StyleGAN Encoder for Improved Reconstruction and Editability

Xudong Mao¹, Liujuan Cao^{2*}, Aurele T. Gnanha³, Zhenguo Yang⁴, Qing Li⁵, Rongrong Ji²

¹Guangdong Key Laboratory of Big Data Analysis and Processing, Sun Yat-sen University, China

²School of Informatics, Xiamen University, China

³Department of Computer Science, City University of Hong Kong, China

⁴Department of Computer Science, Guangdong University of Technology, China

⁵Department of Computing, Hong Kong Polytechnic University, China

maoxd3@mail.sysu.edu.cn, caoliujuan@xmu.edu.cn

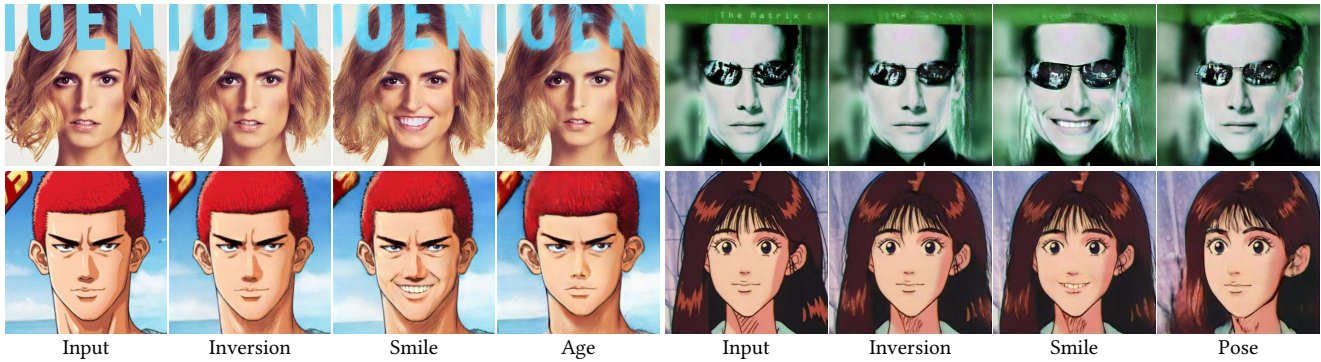


Figure 1: Image editing via our StyleGAN Inversion method. For each example, we show from left to right: the input image, the inverted image, and the edited images using off-the-shelf editing techniques. Our method enables high-quality reconstruction and editing for out-of-domain cartoon images.

ABSTRACT

GAN inversion aims to invert an input image into the latent space of a pre-trained GAN. Despite the recent advances in GAN inversion, there remain challenges to mitigate the tradeoff between distortion and editability, i.e. reconstructing the input image accurately and editing the inverted image with a small visual quality drop. The recently proposed pivotal tuning model makes significant progress towards reconstruction and editability, by using a two-step approach that first inverts the input image into a latent code, called pivot code, and then alters the generator so that the input image can be accurately mapped into the pivot code. Here, we show that both reconstruction and editability can be improved by a proper design of the pivot code. We present a simple yet effective method, named cycle encoding, for a high-quality pivot code. The key idea of our method is to progressively train an encoder in varying spaces according to a cycle scheme: $\mathcal{W} \rightarrow \mathcal{W}^+ \rightarrow \mathcal{W}$. This

*Corresponding author.

Permission to make digital or hard copies of all or part of this work for personal or classroom use is granted without fee provided that copies are not made or distributed for profit or commercial advantage and that copies bear this notice and the full citation on the first page. Copyrights for components of this work owned by others than the author(s) must be honored. Abstracting with credit is permitted. To copy otherwise, or to publish, to post on servers or to redistribute to lists, requires prior specific permission and/or a fee. Request permissions from permissions@acm.org.

MM '22, October 10–14, 2022, Lisboa, Portugal

© 2022 Copyright held by the owner/author(s). Publication rights licensed to ACM.

training methodology preserves the properties of both \mathcal{W} and \mathcal{W}^+ spaces, i.e. high editability of \mathcal{W} and low distortion of \mathcal{W}^+ . To further decrease the distortion, we also propose to refine the pivot code with an optimization-based method, where a regularization term is introduced to reduce the degradation in editability. Qualitative and quantitative comparisons to several state-of-the-art methods demonstrate the superiority of our approach.

CCS CONCEPTS

• **Computing methodologies** → Reconstruction; Image manipulation.

KEYWORDS

GAN, GAN Inversion, Image Manipulation, Cycle Encoding

ACM Reference Format:

Xudong Mao¹, Liujuan Cao^{2*}, Aurele T. Gnanha³, Zhenguo Yang⁴, Qing Li⁵, Rongrong Ji². 2022. Cycle Encoding of a StyleGAN Encoder for Improved Reconstruction and Editability. In *Proceedings of the 30th ACM International Conference on Multimedia (MM '22)*, October 10–14, 2022, Lisboa, Portugal. ACM, New York, NY, USA, 24 pages.

1 INTRODUCTION

In recent years, Generative Adversarial Networks (GANs) [18] have revolutionized unconditional image synthesis. State-of-the-art models, especially StyleGAN [25–27], can now generate realistic and

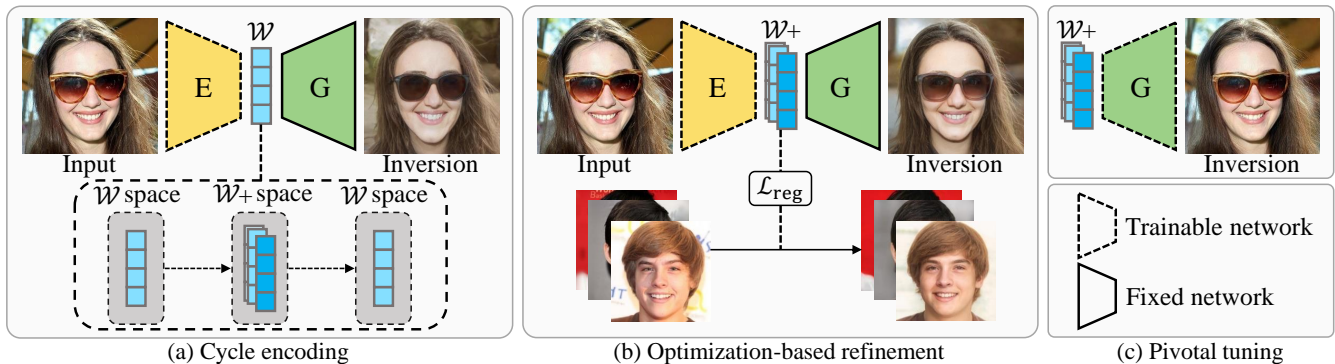


Figure 2: The framework of our StyleGAN inversion method. (a) Cycle encoding: the encoder is trained in varying spaces according to a cycle scheme: $\mathcal{W} \rightarrow \mathcal{W}+ \rightarrow \mathcal{W}$. (b) Optimization-based refinement: the encoder is iteratively updated towards the input image where a regularization term is introduced to prevent overfitting. (c) Pivotal tuning: the generator is slightly tuned so that the input image can be accurately mapped to the latent code.

visually-appealing images in various domains. Furthermore, the intermediate latent space of StyleGAN, which is obtained from the input latent space through a mapping network, has been demonstrated as holding the disentanglement property. Based on this property, there emerges numerous models [1, 4, 12, 27, 36, 41–45, 49, 53, 58] for StyleGAN inversion and real image manipulation.

The target of StyleGAN inversion is to invert an input image into StyleGAN’s latent space. Typically, there are two types of latent spaces for StyleGAN inversion. One is StyleGAN’s native latent space \mathcal{W} [3, 20, 23, 43, 47], where the style code is a 512-dimensional vector, and the other is an extended latent space $\mathcal{W}+$ [1, 2, 41, 49, 62], where the style code consists of 18 different 512-dimensional vectors. It has been shown [6, 42, 49, 64] that the original space \mathcal{W} is more editable while the extended space $\mathcal{W}+$ is more expressive.

Recently, Roich *et al.* [42] propose Pivotal Tuning Inversion (PTI), a two-step approach that achieves significant progress towards reconstruction and editability in StyleGAN inversion. PTI first inverts the input image into a latent code, called pivot code, using an existing per-image optimization inversion method [27], and then slightly alters the generator so that the input image can be accurately mapped to the pivot code. It is revealed [42] that the quality of the pivot code is of crucial importance to the final inversion. To decrease the distortion of the pivot code, one simple method is to apply more training steps during the first step. However, we observe that the per-image optimization method can easily cause overfitting and thereby lead to poor editability.

Instead of using the per-image optimization method, we propose an encoder-based method, named cycle encoding, for a high-quality pivot code. The idea is to preserve the properties of both \mathcal{W} and $\mathcal{W}+$ spaces, by progressively training an encoder according to a cycle scheme: $\mathcal{W} \rightarrow \mathcal{W}+ \rightarrow \mathcal{W}$. Specifically, the encoder starts the training in the \mathcal{W} space, then gradually shifts the space from \mathcal{W} to $\mathcal{W}+$, and finally shifts it back from $\mathcal{W}+$ to \mathcal{W} . We demonstrate that our method yields lower distortion, higher editability, and less inference time compared to PTI.

Recent evidence [19, 62] reveals that the hybrid method exploits the advantages of both encoder-based and optimization-based methods. Inspired by this, we also propose to refine the pivot code obtained in cycle encoding by applying an optimization-based method. Different from existing per-image optimization methods [1, 27] which optimize the latent code directly, our method refines the reconstruction by updating the encoder towards the input image so that an additional regularization term can be used to prevent overfitting. This refinement mechanism decreases the distortion at the cost of a subtle degradation in editability. Figure 2 shows the framework of our approach.

We compare our method with several state-of-the-art StyleGAN inversion methods through qualitative and quantitative evaluation, and demonstrate that our method outperforms these methods in both reconstruction and editability. In Figure 1, we show that our method enables high-quality reconstruction and editing even for out-of-domain cartoon images. Our code is available at <https://github.com/xudonmao/CycleEncoding>.

2 RELATED WORK

2.1 Latent Space Embedding

The high visual quality of GAN synthesis [9, 24, 26, 27] has prompted the researchers to study the latent space of GAN. One fundamental task is GAN inversion [33, 63], where a given image is inverted into the latent space of GAN. In general, GAN inversion methods can typically be divided into three categories [59]: (1) optimization-based methods [1, 2, 13, 14, 16, 22, 27, 30, 32, 40, 48] which directly optimize over the latent code, (2) encoder-based methods [5, 7, 10, 19, 28, 31, 34, 37, 38, 41, 49, 55, 56] which learn an encoder to map the input image into the latent space, and (3) hybrid methods [8, 35, 60, 62, 63] which combine the above two methods. Typically, optimization-based methods achieve lower distortion but take a substantially longer time for computation compared to encoder-based methods. Specifically, Abdal *et al.* [1] optimize the latent code in the extended $\mathcal{W}+$ space and show that even out-of-domain images can be reconstructed. Karras *et al.* [27] perform the optimization over not only the latent code in the original \mathcal{W} space but also

the stochastic noise inputs of the StyleGAN generator. Richardson *et al.* [41] introduce a feature pyramid network architecture for the encoder which encodes the input image into the $\mathcal{W}+$ space. Roich *et al.* [42] propose to first invert the input image into a latent code using the optimization-based method and then slightly alter the generator such that the input image can be accurately mapped to the latent code.

2.2 Latent Space Manipulation

To edit a real image, one may first invert the image into the latent space, and then perform the latent space manipulation techniques. Numerous methods have been proposed to find semantically meaningful directions in the latent space of GANs, where semantic directions can be determined through fully-supervised approaches [3, 17, 43, 50, 57, 65], self-supervised approaches [23, 39, 46, 47], or unsupervised approaches [11, 20, 29, 44, 51, 52, 54]. Specifically, Jahanian *et al.* [23] find semantic directions for camera motion and color transformation in a self-supervised manner. Shen *et al.* [43] use binary facial attribute labels to determine semantic directions. Härkönen *et al.* [20] show that using principal component analysis can identify meaningful semantic directions in an unsupervised manner.

2.3 Distortion-editability Tradeoff

The $\mathcal{W}+$ space is superior in achieving low distortion because it is an enlarged space and thus more expressive. However, recent works [42, 49, 64] show that the \mathcal{W} space obtains better editability than the $\mathcal{W}+$ space, since StyleGAN is originally trained on this space. Tov *et al.* [49] analyze the distortion-editability tradeoff and present an encoder-based method to balance the tradeoff. Zhu *et al.* [64] introduce a new normalized space and a regularization term to address the distortion-editability tradeoff. Roich *et al.* [42] mitigate the distortion-editability tradeoff by combining the editability of the \mathcal{W} space with an accurate reconstruction technique which slightly alters the generator.

3 ANALYSIS OF PIVOTAL TUNING INVERSION

3.1 Pivotal Tuning Inversion

PTI [42] is a two-step method for StyleGAN inversion. Different from previous methods that find the latent code within the StyleGAN’s latent space, PTI augments the latent space by slightly altering the generator. Specifically, in the first step, PTI inverts the input image x into a latent code $w_p \in \mathcal{W}$, called pivot code, using an existing optimization-based method [27] which optimizes the following objective:

$$w_p = \arg \min_{w,n} \mathcal{L}_{\text{LPIPS}}(x, G(w, n)) + \lambda_n \mathcal{L}_n(n), \quad (1)$$

where $G(w, n)$ is the generated image by the generator G , $\mathcal{L}_{\text{LPIPS}}$ is the LPIPS perceptual loss [61], n is a noise vector, \mathcal{L}_n is a noise regularization term, and λ_n controls the weight of \mathcal{L}_n . In the second step, the generator G is tuned so that the input image x can be accurately mapped to the pivot code w_p by optimizing:

$$\mathcal{L}_{\text{PTI}}(x) = \mathcal{L}_{\text{LPIPS}}(x, G(w_p)) + \lambda_{L2} \mathcal{L}_{L2}(x, G(w_p)), \quad (2)$$

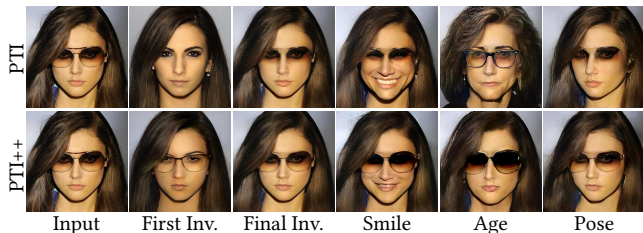


Figure 3: PTI++ denotes the model that is trained with more training steps in the first step (Eq. 1). PTI++ achieves low distortion but poor editability.

where \mathcal{L}_{L2} is the pixel-wise L2 loss and λ_{L2} controls the loss weight.

3.2 Distortion-Editability Tradeoff

Although the distortion can be diminished significantly during the second step of PTI, the distortion in the first step is of crucial importance to the final inversion. Figure 3 shows an example, and one can see that lower distortion in the first step (Column 2) leads to lower distortion of the final inversion (Column 3). One simple method to decrease the distortion is to apply more training steps in the first step (Eq. 1). However, we observe that applying more training steps will decrease the editability of the final inversion, as shown in Figure 3. The reason may be that the per-image optimization method suffers from overfitting when training too many steps on a single image. Therefore, the per-image optimization method for the pivot code can hardly balance the distortion-editability tradeoff. We instead train an encoder using a novel training methodology for the pivot code, resulting in a more accurate, more editable, and faster inversion.

4 METHOD

Our target is to improve the quality of the pivot code in PTI. We adopt the encoder-based method to infer the pivot code, because the per-image optimization method can hardly balance the distortion-editability tradeoff as discussed in Section 3. Recent studies [6, 49, 64] reveal that the extended space $\mathcal{W}+$ is more expressive while the original space \mathcal{W} is more editable. The key idea of our method is to exploit the advantages of both $\mathcal{W}+$ and \mathcal{W} spaces by training an encoder in both spaces. We propose a novel training methodology that gradually changes the output space of the encoder according to a cycle scheme: $\mathcal{W} \rightarrow \mathcal{W}+ \rightarrow \mathcal{W}$. To further decrease the distortion, we then follow the hybrid method [19, 62] to refine the pivot code obtained from the encoder, by iteratively updating the encoder towards the input image where a regularization term is introduced to alleviate the overfitting problem. Finally, using the latent code obtained from cycle encoding or from the refinement as the pivot code, the generator is slightly tuned so that the input image can be accurately mapped to the pivot code. Figure 2 shows the framework of our method.

4.1 Cycle Encoding

In cycle encoding, we seek to achieve optimal editability for the pivot code. To this end, we select the \mathcal{W} space as the final state for cycle encoding, as the \mathcal{W} space provides better editability than the



Figure 4: Reconstruction quality comparison on CelebA-HQ.

$\mathcal{W}+$ space [49]. Nevertheless, the $\mathcal{W}+$ space is more expressive and induces less distortion. To exploit both advantages of the \mathcal{W} and $\mathcal{W}+$ spaces, we propose to train an encoder in varying spaces according to a cycle scheme: $\mathcal{W} \rightarrow \mathcal{W}+ \rightarrow \mathcal{W}$. Starting and ending with the \mathcal{W} space provide high editability for the pivot code, and shifting to the $\mathcal{W}+$ space provides high expressiveness for the pivot code. For $\mathcal{W} \rightarrow \mathcal{W}+$, we follow [49] to sequentially allow the latent vectors to be different to the first latent vector. For $\mathcal{W}+ \rightarrow \mathcal{W}$, it is more crucial to the final inversion, as it determines the final state of the pivot code. We propose a new progressive training methodology for $\mathcal{W}+ \rightarrow \mathcal{W}$, which changes the space more smoothly. In the following, we detail the training mechanism that consists of two steps:

4.1.1 $\mathcal{W} \rightarrow \mathcal{W}+$.

We follow the e4e model [49] to control the output space of the encoder by using the delta regularization loss which measures the difference between each latent vector. Formally, let $E(x) = (w_0, w_1, \dots, w_{N-1}) = (w_0, w_0 + \Delta_1, \dots, w_0 + \Delta_{N-1})$ denote the output of the encoder, where N is the number of the latent vectors and Δ_i is the offset from the first latent vector w_0 . The delta regularization loss is defined as:

$$\mathcal{L}_{\text{delta}}(x) = \sum_{i=1}^{N-1} \|\Delta_i\|_2. \quad (3)$$

The encoder starts the training in the \mathcal{W} space by setting $\forall i : \Delta_i = 0$, and then gradually shifts the space from \mathcal{W} to $\mathcal{W}+$ by training Δ_i sequentially every T_0 iterations.

4.1.2 $\mathcal{W}+ \rightarrow \mathcal{W}$.

In this step, we also utilize the delta regularization loss to control the shift from $\mathcal{W}+$ to \mathcal{W} . We empirically find that smoothly changing the output space of the encoder is beneficial to the editability of the pivot code. To this end, we propose a new progressive training methodology that shifts the space from $\mathcal{W}+$ to \mathcal{W} more smoothly. Specifically, we first gradually increase the weight of the delta regularization loss by a factor β every T_1 iterations. A large weight of the delta regularization loss enforces Δ_i to be very close to 0. After this procedure, the output space of the encoder lies close to the \mathcal{W} space with a small variance. Then, we set from $\Delta_{N-1} = 0$



Figure 5: Reconstruction quality comparison using famous character images.

to $\Delta_1 = 0$ sequentially every T_2 iterations. Finally, the output space of the encoder ends at the \mathcal{W} space with $\forall i : \Delta_i = 0$.

Increasing the weight of the delta regularization loss can be viewed as a “soft” operation, and setting $\Delta_i = 0$ can be viewed as a “hard” operation. In short, our progressive training methodology first performs the soft operation and then performs the hard operation. Compared with directly performing the hard operation, our method changes the output space of the encoder more smoothly and favors better property preservation of the \mathcal{W} and $\mathcal{W}+$ spaces.

The overall objective of cycle encoding is:

$$\mathcal{L}(x) = \lambda_{L2} \mathcal{L}_{L2}(x) + \lambda_{\text{lpiips}} \mathcal{L}_{\text{LPIPS}}(x) + \lambda_{\text{id}} \mathcal{L}_{\text{ID}}(x) + \lambda_{\text{adv}} \mathcal{L}_{\text{adv}}(x) + \lambda_{\text{delta}} \mathcal{L}_{\text{delta}}(x), \quad (4)$$

where \mathcal{L}_{ID} is the identity loss [15], \mathcal{L}_{adv} [34, 49] is an adversarial loss to encourage w_i to lie close to the true distribution of \mathcal{W} , and λ controls the weight of each loss.

4.2 Decreasing Distortion via Optimization

The hybrid method [19, 62] has proved the effectiveness of utilizing the optimization-based method to refine the output of the encoder. Inspired by this, we also explore applying optimization to the result of cycle encoding to further decrease the distortion. However, as we discussed in Section 3, optimizing over a single image is prone to overfitting, which then decreases the editability. Instead of optimizing the latent code, our method iteratively updates the encoder towards the input image where a regularization term is introduced to alleviate the overfitting problem. At each iteration, we randomly sample M images x^* from the training set and apply the following regularization term:

$$\mathcal{L}_{\text{reg}}(x^*) = \frac{1}{M} \sum_{i=0}^{M-1} \mathcal{L}_{\text{S}}(x_i^*, G(E(x_i^*))), \quad (5)$$

where $\mathcal{L}_{\text{S}} = \lambda_{L2} \mathcal{L}_{L2} + \lambda_{\text{lpiips}} \mathcal{L}_{\text{LPIPS}} + \lambda_{\text{id}} \mathcal{L}_{\text{ID}}$. Then, the overall objective of this optimization step is:

$$\mathcal{L}_{\text{ref}}(x, x^*) = \mathcal{L}_{\text{S}}(x) + \lambda_{\text{reg}} \mathcal{L}_{\text{reg}}(x^*), \quad (6)$$

where x is the input image and λ_{reg} controls the loss weight. Moreover, we apply this optimization in the $\mathcal{W}+$ space, as we empirically



Figure 6: Reconstruction quality comparison using cartoon images.



Figure 7: Reconstruction quality comparison of the pivot code.

find that learning in the $\mathcal{W}+$ space in this step is cost-effective in decreasing the distortion with a subtle degradation in editability. The reason may be that slight and local changes to the pivot code can be applied without damaging its editing capability.

Note that this optimization step is optional in practice, and we recommend applying this step for challenging images as skipping this step reduces the inference time. Furthermore, a small number (15 in our experiments) of iterations is sufficient, since the reconstruction quality of cycle encoding is already quite good.

5 EXPERIMENTS

In this section, we evaluate the effectiveness of our inversion method in terms of reconstruction and editing quality. For all experiments, we use a StyleGAN2 [27] generator pre-trained on the FFHQ [26] dataset.

Datasets. We train our model on the FFHQ [26] dataset which contains 70,000 facial images. The CelebA-HQ [24] test set is used for evaluation. Furthermore, we collect 200 challenging facial images from the web for evaluation, including famous character images and cartoon images.

Baselines. We compare our method with four well-known inversion methods: SG2 [27], SG2 $\mathcal{W}+$ [1], e4e [49], and PTI [42]. SG2

Table 1: Quantitative reconstruction quality on CelebA-HQ.

Method	Identity \uparrow	LPIPS \downarrow	MSE \downarrow	Runtime \downarrow
SG2 [27]	0.193	0.373	0.099	48.91
SG2 $\mathcal{W}+$ [1]	0.667	0.279	0.041	162.3
e4e [49]	0.494	0.392	0.053	0.089
PTI [42]	0.845	0.101	0.013	102.2
Cycle	0.855	0.095	0.011	67.47
Cycle+Optim.	0.866	0.093	0.011	80.81

Table 2: Quantitative reconstruction quality on 200 challenging images collected from the web.

Method	Identity \uparrow	LPIPS \downarrow	MSE \downarrow	Runtime \downarrow
PTI [42]	0.774	0.146	0.022	102.7
Cycle	0.820	0.120	0.018	67.70
Cycle+Optim.	0.843	0.116	0.017	81.09

Table 3: Quantitative reconstruction quality of the pivot code on CelebA-HQ.

Method	Identity \uparrow	LPIPS \downarrow	MSE \downarrow	Runtime \downarrow
PTI [42]	0.179	0.377	0.099	35.85
Cycle	0.343	0.415	0.066	0.043
Cycle+Optim.	0.514	0.377	0.047	13.34

and SG2 $\mathcal{W}+$ are optimization-based methods that invert the input images into the \mathcal{W} and $\mathcal{W}+$ spaces, respectively. The e4e model is an encoder-based method that extends the psp model [41] by encouraging the latent codes close to \mathcal{W} . PTI is a two-step method that first infers the latent code using SG2 and then slightly alters the generator to fit the latent code. The qualitative comparison to SG2 $\mathcal{W}+$ is provided in the Supplementary Materials due to the limited space.

5.1 Implementation Details

In the step of $\mathcal{W} \rightarrow \mathcal{W}+$, we train the encoder for 500K iterations using the same hyperparameters as described in [49]. In the step of $\mathcal{W}+ \rightarrow \mathcal{W}$, we train the encoder for 250K iterations. Specifically, in the first 150K iterations, we gradually increase λ_{delta} (Eq. 4) by 20% and decrease λ_{adv} (Eq. 4) by 50% every 10K iterations. Then, we set from $\Delta_{N-1} = 0$ to $\Delta_1 = 0$ sequentially every 4K iterations. For the regularized refinement step, we randomly sample 7 images from the FFHQ training set and update the encoder for 15 iterations. For the loss weights in Eq. 5-6, we set $\lambda_{L2} = 1$, $\lambda_{\text{lpips}} = 0.8$, $\lambda_{\text{id}} = 0.1$, and $\lambda_{\text{reg}} = 1$. For the pivotal tuning step, we use the same hyperparameters as described in [42]. For the quantitative experiments, we follow [42] to evaluate the models on the first 1000 samples from the CelebA-HQ test set. All experiments are performed using a single Nvidia GeForce RTX 3090 GPU.

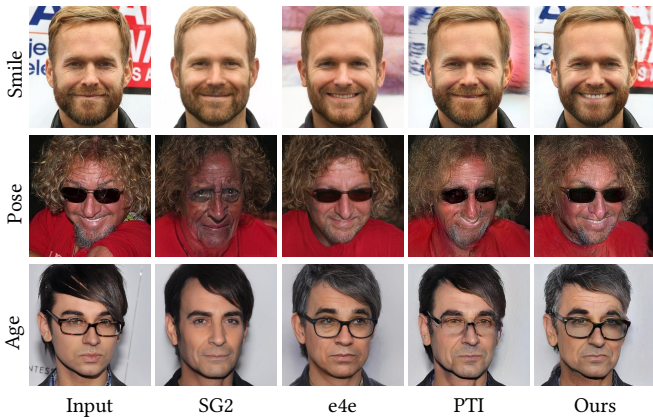


Figure 8: Editing quality comparison on CelebA-HQ. In each example, the editing is performed using the same editing weight.

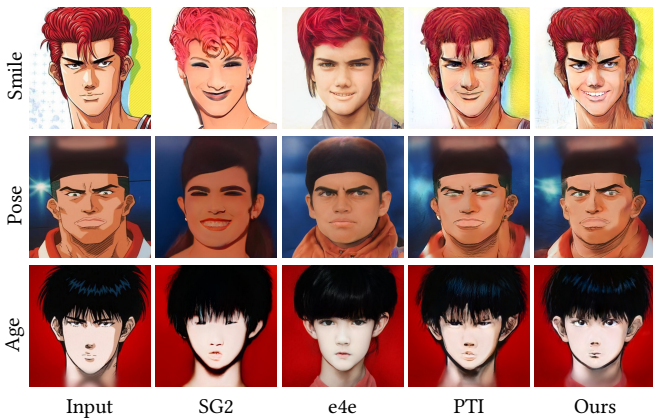


Figure 9: Editing quality comparison using cartoon images. In each example, the editing is performed using the same editing weight.

5.2 Reconstruction Quality

Qualitative Evaluation. Figures 4 to 6 present a visually qualitative comparison of the reconstructed images. The results show that our method achieves superior reconstruction for all images from three different data sources. Figures 4 and 5 show that the reconstruction obtained by our method preserves more accurate details, such as cap (row 1, Figure 4), background (row 2, Figure 4), hand (row 1, Figure 5), and makeup (row 3, Figure 5). Figure 6 presents the reconstruction of cartoon images. Inverting cartoon images is more challenging as the cartoon images are completely out-of-domain. In Figure 6, the reconstructed images by PTI tend to be blurry, and some key components (e.g., eye and mouth) are not accurately reconstructed. In contrast, our method successfully reconstructs the cartoon images. Examples of using cycle encoding only (i.e., without applying the optimization step) are provided

Table 4: Quantitative editing quality by evaluating the editing magnitude (e.g., rotation angle) when applying the same editing weight α .

Rotation Angle \uparrow	$\alpha = 1$	$\alpha = 5$	$\alpha = 10$
SG2 [27]	3.83	16.70	32.68
SG2 \mathcal{W}^+ [1]	2.48	10.74	21.72
e4e [49]	3.49	14.90	29.13
PTI [42]	3.44	16.64	33.09
Ours	4.63	22.20	42.54

Table 5: Quantitative editing quality by evaluating the identity similarity when applying the same editing magnitude (e.g., rotation angle).

Identity \uparrow	Angle ± 5	Angle ± 10	Angle ± 15
SG2 [27]	0.188	0.179	0.166
SG2 \mathcal{W}^+ [1]	0.621	0.538	0.454
e4e [49]	0.487	0.471	0.442
PTI [42]	0.778	0.673	0.565
Ours	0.812	0.728	0.638

in Figure 11, and one can see that cycle encoding already outperforms PTI in reconstruction. More visual results are provided in the Supplementary Materials.

Quantitative Evaluation. Table 1 presents a quantitative evaluation among different inversion methods. We employ three metrics, including identity similarity score [21], LPIPS [61], and Mean Squared Error (MSE)¹. Following [41], we measure the identity similarity score by using a different face recognition model (Curricularface [21]) to make the similarity score independent from the loss function (ArcFace [15]). The results demonstrate that our method achieves the best reconstruction quality in terms of all three metrics. Our method reduces the inference time of PTI from 102.2 seconds to 80.8 seconds. Without applying the optimization step, the inference time can be further reduced to 67.5 seconds. Moreover, we also evaluate the models on 200 challenging images collected from the web. In Table 2, we see a substantial improvement over PTI from 0.774 to 0.843 in identity similarity.

Pivot Code Quality. Here, we evaluate the reconstruction quality of the pivot code. Figure 7 presents the reconstructed results of the pivot code using examples in Figures 4 to 6. One can see that our method achieves significantly lower distortion compared to PTI, especially for the challenging cartoon images. The quantitative results in Table 3 also demonstrate that our method outperforms PTI by a substantial margin.

5.3 Editing Quality

In addition to reconstruction quality, editing quality is another important target for GAN inversion, as the major motivation for GAN inversion is the downstream editing task. Several works [42, 49, 64] have discussed the editing quality, and they show that the native \mathcal{W}

¹The implementation of identity similarity score, LPIPS, and MSE is from <https://github.com/eladrich/pixel2style2pixel>.



Figure 10: Editing quality comparison using famous character images. In each example, the editing is performed using the same editing weight.

space is superior to the extended $\mathcal{W}+$ space in terms of editability. A high editability is expected that given the inverted latent code, one can edit it and obtain the desired editing magnitude with a small reconstruction accuracy drop. In the following experiments, we use the popular editing method, InterfaceGAN [43], for latent-based editing. InterfaceGAN edits the original latent code z with $z_{edit} = z + \alpha n$, where α is the editing weight and n is a unit normal vector, corresponding to a semantic direction. One can see that the reconstruction quality will decrease as the editing weight α increases, since αn will dominate the value of z_{edit} when α is large. Thus we also expect to obtain the desired editing magnitude with a small editing weight α . Based on the above observations, we follow [42] to evaluate the editing quality by using two metrics: *editing magnitude* when applying the same editing weight, and *identity preservation* when applying the same editing magnitude.

Qualitative Evaluation. In Figures 8 to 10, we provide a qualitative comparison of different methods in editing images. To compare the editing magnitude, in each example, the edited images by different methods are obtained using the same editing weight α . As can

be seen in Figures 8 and 10, our method achieves the largest editing magnitude for all the examples, and our method provides the best visually-pleasing editing results and most accurately preserves the identity of the input images. For example, PTI loses the identity and details, such as background (row 1, Figure 8), appearance (row 2, Figure 8), eyes (row 2, Figure 10), and glasses (row 3, Figure 10). SG2 and e4e achieve visually-pleasing editing quality but lose the identity of the input images. We also investigate the performance of our method on more challenging out-of-domain cartoon images in Figure 9. The edited images by PTI tend to be blurry. Our method is the only one that successfully reconstructs and edits the cartoon images. For more editing results, more editing directions, and editing results using StyleClip [36], see the Supplementary Materials.

Quantitative Evaluation. Tables 4 and 5 present a quantitative comparison of different methods. As aforementioned, we use *editing magnitude* and *identity preservation* to measure the editing quality. We follow [42, 64] to use the pose editing operation for this evaluation, as evaluating the rotation angle is more accurate than the other operations. Microsoft Face API is used to calculate

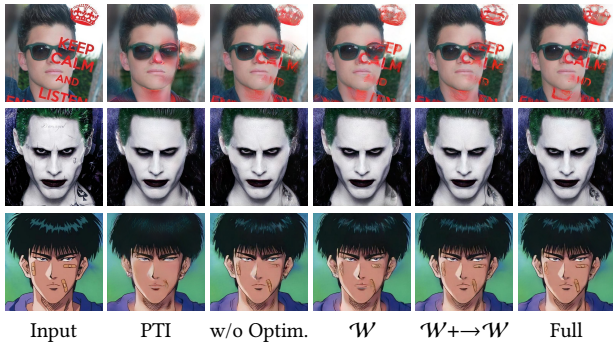


Figure 11: Ablation study. The full model achieves the best reconstruction quality.

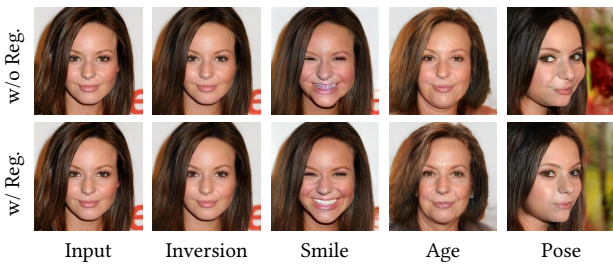


Figure 12: Ablation study of the regularization, where the editing is performed using the same editing weight. Without the regularization, the model yields inferior editability.

the rotation angle. As shown in Table 4, our method induces the largest rotation angle compared to the baselines, especially when the editing weight is large. In Table 5, our method also achieves the best score in terms of identity similarity, which indicates that our method most accurately preserves the identity of the original images when performing the same editing magnitude. For the case of Angle ± 15 , we see a substantial editing quality improvement over PTI from 0.565 to 0.638.

5.4 Ablation Study

Optimization-based Refinement. We first perform an ablation study on the optimization step described in Section 4.2. We compare our model with two variants: skipping the optimization step (denoted as w/o Optim.) and removing the regularization term (w/o Reg.). The quantitative results in Table 6 demonstrate that the optimization step decreases the distortion with a subtle drop in editability, and the regularization term alleviates the drop in editability. The qualitative examples in Figure 11 and 12 show consistent results with the quantitative evaluation. Note that without the optimization step, cycle encoding already outperforms PTI in both reconstruction and editability.

Cycle Encoding. We then perform an ablation study on the cycle encoding step. We compare our model with three variants: training the encoder in \mathcal{W} , training the encoder in $\mathcal{W} \rightarrow \mathcal{W}+$, and training the encoder in $\mathcal{W}+ \rightarrow \mathcal{W}$. The details of the model configurations can be found in the Supplementary Materials, and all the models are

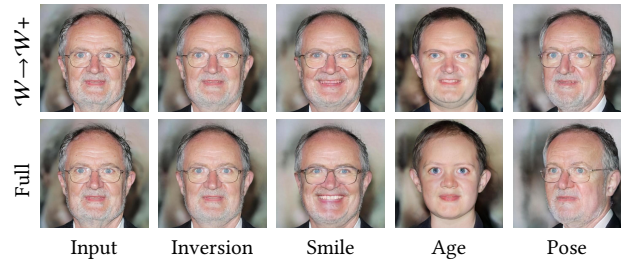


Figure 13: Ablation study of cycle encoding, where the editing is performed using the same editing weight. $\mathcal{W} \rightarrow \mathcal{W}+$ yields inferior editability.

Table 6: Ablation study of the optimization step. First row: reconstruction evaluation via identity similarity. Second row: editability evaluation via rotation angle.

	PTI [42]	w/o Optim.	w/o Reg.	Full
Identity \uparrow	0.845	0.855	0.869	0.866
Angle \uparrow	16.64	22.49	19.95	22.20

Table 7: Ablation study of cycle encoding. First row: reconstruction evaluation via identity similarity. Second row: editability evaluation via rotation angle.

	\mathcal{W}	$\mathcal{W} \rightarrow \mathcal{W}+$	$\mathcal{W}+ \rightarrow \mathcal{W}$	Full
Identity \uparrow	0.849	0.875	0.859	0.866
Angle \uparrow	16.33	14.70	21.24	22.20

trained for the same number of iterations. The quantitative results in Table 7 show that $\mathcal{W} \rightarrow \mathcal{W}+$ achieves the lowest distortion but poorest editability. Figure 13 also demonstrates that cycle encoding achieves superior editability than $\mathcal{W} \rightarrow \mathcal{W}+$. For $\mathcal{W}+ \rightarrow \mathcal{W}$, we observe a slight degeneration in both reconstruction and editability compared to cycle encoding from Figure 11 and Table 7. \mathcal{W} behaves poorly in both reconstruction and editability.

6 DISCUSSION AND CONCLUSION

In this work, we propose a StyleGAN inversion method, named cycle encoding, for a high-quality pivot code in PTI. We demonstrate the superior performance of our method in both reconstruction and editability compared to several state-of-the-art methods. Our method even enables high-quality reconstruction and editing for out-of-domain cartoon images. Although our model successfully reconstructs the presented cartoon examples, it can hardly reconstruct more cartoonized images. In the future, we plan to develop a model with stronger generalization ability, so as to invert more challenging images from different domains such as cartoons and sketches.

7 ACKNOWLEDGEMENT

This work is supported by the National Natural Science Foundation of China (No.62176223).

REFERENCES

- [1] Rameen Abdal, Yipeng Qin, and Peter Wonka. 2019. Image2stylegan: How to embed images into the stylegan latent space?. In *Proceedings of International Conference on Computer Vision*.
- [2] Rameen Abdal, Yipeng Qin, and Peter Wonka. 2020. Image2StyleGAN++: How to Edit the Embedded Images?. In *Proceedings of IEEE Conference on Computer Vision and Pattern Recognition*.
- [3] Rameen Abdal, Peihao Zhu, Niloy J. Mitra, and Peter Wonka. 2021. StyleFlow: Attribute-Conditioned Exploration of StyleGAN-Generated Images Using Conditional Continuous Normalizing Flows. *ACM Transactions on Graphics* 40, 3 (2021).
- [4] Shady Abu Hussein, Tom Tirer, and Raja Giryes. 2020. Image-Adaptive GAN based Reconstruction. In *Proceedings of AAAI Conference*.
- [5] Yuval Alaluf, Or Patashnik, and Daniel Cohen-Or. 2021. Only a Matter of Style: Age Transformation Using a Style-Based Regression Model. *arXiv preprint arXiv:2102.02754* (2021).
- [6] Yuval Alaluf, Or Patashnik, and Daniel Cohen-Or. 2021. ReStyle: A Residual-Based StyleGAN Encoder via Iterative Refinement. *arXiv preprint arXiv:2104.02699* (2021).
- [7] David Bau, Hendrik Strobelt, William Peebles, Jonas Wulff, Bolei Zhou, Jun-Yan Zhu, and Antonio Torralba. 2019. Semantic photo manipulation with a generative image prior. *ACM Transactions on Graphics* 38, 4 (2019).
- [8] Baylies. 2019. <https://github.com/pbaylies/stylegan-encoder>.
- [9] Andrew Brock, Jeff Donahue, and Karen Simonyan. 2018. Large Scale GAN Training for High Fidelity Natural Image Synthesis. In *Proceedings of International Conference on Learning Representations*.
- [10] Lucy Chai, Jonas Wulff, and Phillip Isola. 2021. Using latent space regression to analyze and leverage compositionality in GANs. In *Proceedings of International Conference on Learning Representations*.
- [11] Anton Cherepov, Andrey Voynov, and Artem Babenko. 2021. Navigating the GAN Parameter Space for Semantic Image Editing. In *Proceedings of IEEE Conference on Computer Vision and Pattern Recognition*.
- [12] Min Jin Chong, Hsin-Ying Lee, and David Forsyth. 2021. StyleGAN of All Trades: Image Manipulation with Only Pretrained StyleGAN. *arXiv preprint arXiv:2111.01619* (2021).
- [13] Edo Collins, Raja Bala, Bob Price, and Sabine Susstrunk. 2020. Editing in Style: Uncovering the Local Semantics of GANs. In *Proceedings of IEEE Conference on Computer Vision and Pattern Recognition*.
- [14] Antonia Creswell and Anil Anthony Bharath. 2018. Inverting the generator of a generative adversarial network. *IEEE Transactions on Neural Networks and Learning Systems* 30, 7 (2018), 1967–1974.
- [15] Jiankang Deng, Jia Guo, Niannan Xue, and Stefanos Zafeiriou. 2019. Arcface: Additive angular margin loss for deep face recognition. In *Proceedings of IEEE Conference on Computer Vision and Pattern Recognition*.
- [16] David Futschik, Michal Lukáč, Eli Shechtman, and Daniel Šýkora. 2021. Real Image Inversion via Segments. *arXiv preprint arXiv:2110.06269* (2021).
- [17] Lore Goetschalckx, Alex Andonian, Aude Oliva, and Phillip Isola. 2019. GANalyze: Toward Visual Definitions of Cognitive Image Properties. In *Proceedings of International Conference on Computer Vision*.
- [18] Ian Goodfellow, Jean Pouget-Abadie, Mehdi Mirza, Bing Xu, David Warde-Farley, Sherjil Ozair, Aaron Courville, and Yoshua Bengio. 2014. Generative Adversarial Nets. In *Proceedings of Neural Information Processing Systems*, Vol. 27.
- [19] Shanyan Guan, Ying Tai, Bingbing Ni, Feida Zhu, Feiyue Huang, and Xiaokang Yang. 2020. Collaborative Learning for Faster StyleGAN Embedding. *arXiv preprint arXiv:2007.01758* (2020).
- [20] Erik Härkönen, Aaron Hertzmann, Jaakko Lehtinen, and Sylvain Paris. 2020. GANSpace: Discovering Interpretable GAN Controls. In *Proceedings of Neural Information Processing Systems*.
- [21] Yuge Huang, Yuhang Wang, Ying Tai, Xiaoming Liu, Pengcheng Shen, Shaoxin Li, Jilin Li, and Feiyue Huang. 2020. CurricularFace: Adaptive Curriculum Learning Loss for Deep Face Recognition. In *Proceedings of IEEE Conference on Computer Vision and Pattern Recognition*.
- [22] Minyoung Huh, Richard Zhang, Jun-Yan Zhu, Sylvain Paris, and Aaron Hertzmann. 2020. Transforming and Projecting Images into Class-conditional Generative Networks. In *Proceedings of European Conference on Computer Vision*.
- [23] Ali Jahani, Lucy Chai, and Phillip Isola. 2020. On the "steerability" of generative adversarial networks. In *Proceedings of International Conference on Learning Representations*.
- [24] Tero Karras, Timo Aila, Samuli Laine, and Jaakko Lehtinen. 2018. Progressive growing of gans for improved quality, stability, and variation. In *Proceedings of International Conference on Learning Representations*.
- [25] Tero Karras, Miika Aittala, Janne Hellsten, Samuli Laine, Jaakko Lehtinen, and Timo Aila. 2020. Training Generative Adversarial Networks with Limited Data. In *Proceedings of Neural Information Processing Systems*.
- [26] Tero Karras, Samuli Laine, and Timo Aila. 2019. A style-based generator architecture for generative adversarial networks. In *Proceedings of IEEE Conference on Computer Vision and Pattern Recognition*.
- [27] Tero Karras, Samuli Laine, Miika Aittala, Janne Hellsten, Jaakko Lehtinen, and Timo Aila. 2020. Analyzing and improving the image quality of stylegan. In *Proceedings of IEEE Conference on Computer Vision and Pattern Recognition*.
- [28] Hyunsoo Kim, Yunjeong Choi, Junho Kim, Sungjoo Yoo, and Youngjung Uh. 2021. Exploiting Spatial Dimensions of Latent in GAN for Real-time Image Editing. In *Proceedings of IEEE Conference on Computer Vision and Pattern Recognition*.
- [29] Guanyue Li, Yi Liu, Xiwen Wei, Yang Zhang, Si Wu, Yong Xu, and Hau-San Wong. 2021. Discovering Density-Preserving Latent Space Walks in GANs for Semantic Image Transformations. In *Proceedings of ACM International Conference on Multimedia*.
- [30] Zachary C Lipton and Subarna Tripathi. 2017. Precise recovery of latent vectors from generative adversarial networks. In *Proceedings of International Conference on Learning Representations Workshops*.
- [31] Junyu Luo, Yong Xu, Chenwei Tang, and Jiancheng Lv. 2017. Learning Inverse Mapping by AutoEncoder Based Generative Adversarial Nets. In *Proceedings of Neural Information Processing Systems*.
- [32] Sachit Menon, Alexandru Damian, Shijia Hu, Nikhil Ravi, and Cynthia Rudin. 2020. PULSE: Self-Supervised Photo Upsampling via Latent Space Exploration of Generative Models. In *Proceedings of IEEE Conference on Computer Vision and Pattern Recognition*.
- [33] Anh Nguyen, Alexey Dosovitskiy, Jason Yosinski, Thomas Brox, and Jeff Clune. 2016. Synthesizing the preferred inputs for neurons in neural networks via deep generator networks. In *Proceedings of Neural Information Processing Systems*.
- [34] Yotam Nitzan, A. Bermanno, Yangyan Li, and D. Cohen-Or. 2020. Face identity disentanglement via latent space mapping. *ACM Transactions on Graphics* 39 (2020), 1 – 14.
- [35] Xingang Pan, Xiaohang Zhan, Bo Dai, Dahua Lin, Chen Change Loy, and Ping Luo. 2020. Exploiting deep generative prior for versatile image restoration and manipulation. In *Proceedings of European Conference on Computer Vision*.
- [36] Or Patashnik, Zongze Wu, Eli Shechtman, Daniel Cohen-Or, and Dani Lischinski. 2021. StyleCLIP: Text-Driven Manipulation of StyleGAN Imagery. In *Proceedings of International Conference on Computer Vision*.
- [37] Guim Perarnau, Joost Van De Weijer, Bogdan Raducanu, and Jose M Álvarez. 2016. Invertible conditional gans for image editing. *arXiv preprint arXiv:1611.06355* (2016).
- [38] Stanislav Pidhorskiy, Donald Adjeroh, and Gianfranco Doretto. 2020. Adversarial Latent Autoencoders. In *Proceedings of IEEE Conference on Computer Vision and Pattern Recognition*.
- [39] Antoine Plummerault, Hervé Le Borgne, and Céline Hudelot. 2020. Controlling generative models with continuous factors of variations. In *Proceedings of International Conference on Learning Representations*.
- [40] Ankit Raj, Yuqi Li, and Yoram Bresler. 2019. GAN-based Projector for Faster Recovery with Convergence Guarantees in Linear Inverse Problems. In *Proceedings of International Conference on Computer Vision*.
- [41] Elad Richardson, Yuval Alaluf, Or Patashnik, Yotam Nitzan, Yaniv Azar, Stav Shapiro, and Daniel Cohen-Or. 2021. Encoding in Style: a StyleGAN Encoder for Image-to-Image Translation. In *Proceedings of IEEE Conference on Computer Vision and Pattern Recognition*.
- [42] Daniel Roich, Ron Mokady, Amit H. Bermanno, and Daniel Cohen-Or. 2021. Pivotal Tuning for Latent-based Editing of Real Images. *arXiv preprint arXiv:2106.05744* (2021).
- [43] Yujun Shen, Jinjin Gu, Xiaoou Tang, and Bolei Zhou. 2020. Interpreting the latent space of gans for semantic face editing. In *Proceedings of IEEE Conference on Computer Vision and Pattern Recognition*.
- [44] Yujun Shen and Bolei Zhou. 2021. Closed-Form Factorization of Latent Semantics in GANs. In *Proceedings of IEEE Conference on Computer Vision and Pattern Recognition*.
- [45] Mustafa Shukor, Xu Yao, Bharath Bhushan Damodaran, and Pierre Hellier. 2021. Semantic and Geometric Unfolding of StyleGAN Latent Space. *arXiv preprint arXiv:2107.04481* (2021).
- [46] Nurit Spingarn-Eliezer, Ron Banner, and Tomer Michaeli. 2021. GAN Steerability without optimization. In *Proceedings of International Conference on Learning Representations*.
- [47] Ayush Tewari, Mohamed Elgharib, Gaurav Bharaj, Florian Bernard, Hans-Peter Seidel, Patrick Pérez, Michael Zollhöfer, and Christian Theobalt. 2020. StyleRig: Rigging StyleGAN for 3D Control over Portrait Images. *arXiv preprint arXiv:2004.00121* (2020).
- [48] Ayush Tewari, Mohamed Elgharib, Mallikarjun B R., Florian Bernard, Hans-Peter Seidel, Patrick Pérez, Michael Zollhöfer, and Christian Theobalt. 2020. PIE: Portrait Image Embedding for Semantic Control. *ACM Transactions on Graphics* 39, 6 (2020).
- [49] Omer Tov, Yuval Alaluf, Yotam Nitzan, Or Patashnik, and Daniel Cohen-Or. 2021. Designing an Encoder for StyleGAN Image Manipulation. *ACM Transactions on Graphics* 40, 4 (2021).
- [50] Yuri Viazovetskiy, Vladimir Ivashkin, and Evgeny Kashin. 2020. StyleGAN2 Distillation for Feed-forward Image Manipulation. In *Proceedings of European Conference on Computer Vision*.

- [51] Andrey Voynov and Artem Babenko. 2020. Unsupervised discovery of interpretable directions in the gan latent space. In *Proceedings of International Conference on Machine Learning*.
- [52] Binxu Wang and Carlos R. Ponce. 2021. The Geometry of Deep Generative Image Models and its Applications. In *Proceedings of International Conference on Learning Representations*.
- [53] Hao Wang, Guosheng Lin, Steven C. H. Hoi, and Chunyan Miao. 2021. Cycle-Consistent Inverse GAN for Text-to-Image Synthesis. In *Proceedings of ACM International Conference on Multimedia*.
- [54] Hui-Po Wang, Ning Yu, and Mario Fritz. 2021. Hijack-GAN: Unintended-Use of Pretrained, Black-Box GANs. In *Proceedings of IEEE Conference on Computer Vision and Pattern Recognition*.
- [55] Tengfei Wang, Yong Zhang, Yanbo Fan, Jue Wang, and Qifeng Chen. 2021. High-Fidelity GAN Inversion for Image Attribute Editing. *arXiv preprint arXiv:2109.06590* (2021).
- [56] Tianyi Wei, Dongdong Chen, Wenbo Zhou, Jing Liao, Weiming Zhang, Lu Yuan, Gang Hua, and Nenghai Yu. 2021. A Simple Baseline for StyleGAN Inversion. *arXiv preprint arXiv:2104.07661* (2021).
- [57] Zongze Wu, Dani Lischinski, and Eli Shechtman. 2021. StyleSpace Analysis: Disentangled Controls for StyleGAN Image Generation. In *Proceedings of IEEE Conference on Computer Vision and Pattern Recognition*.
- [58] Zongze Wu, Yotam Nitzan, Eli Shechtman, and Dani Lischinski. 2021. StyleAlign: Analysis and Applications of Aligned StyleGAN Models. *arXiv preprint arXiv:2110.11323* (2021).
- [59] Weihao Xia, Yulun Zhang, Yujiu Yang, Jing-Hao Xue, Bolei Zhou, and Ming-Hsuan Yang. 2021. GAN Inversion: A Survey. *arXiv preprint arXiv:2101.05278* (2021).
- [60] Lingyun Zhang, Xiuxiu Bai, and Yao Gao. 2021. Sals-GAN: Spatially-Adaptive Latent Space in StyleGAN for Real Image Embedding. In *Proceedings of ACM International Conference on Multimedia*.
- [61] Richard Zhang, Phillip Isola, Alexei A. Efros, Eli Shechtman, and Oliver Wang. 2018. The Unreasonable Effectiveness of Deep Features as a Perceptual Metric. In *Proceedings of IEEE Conference on Computer Vision and Pattern Recognition*.
- [62] Jiapeng Zhu, Yujun Shen, Deli Zhao, and Bolei Zhou. 2020. In-domain gan inversion for real image editing. In *Proceedings of European Conference on Computer Vision*.
- [63] Jun-Yan Zhu, Philipp Krähenbühl, Eli Shechtman, and Alexei A Efros. 2016. Generative visual manipulation on the natural image manifold. In *Proceedings of European Conference on Computer Vision*.
- [64] Peihao Zhu, Rameen Abdal, Yipeng Qin, and Peter Wonka. 2020. Improved StyleGAN Embedding: Where are the Good Latents? *arXiv preprint arXiv:2012.09036* (2020).
- [65] Peiye Zhuang, Oluwasanmi Koyejo, and Alexander G. Schwing. 2021. Enjoy Your Editing: Controllable GANs for Image Editing via Latent Space Navigation. In *Proceedings of International Conference on Learning Representations*.

Appendices

A ADDITIONAL VISUAL RESULTS

Figures 16 to 24 present additional reconstruction and editing results using images from CelebA-HQ test set, famous character images, and cartoon images.

B MORE EDITING DIRECTIONS

Figures 25 and 26 present the editing results using more directions², including eyes open/close, eye and eyebrow distance, and lip ratio.

C EDITING WITH STYLECLIP

Figures 27 and 28 present the editing results using StyleClip [36], including hairstyle edits and celebrity edits.

D OPTIMIZATION IN \mathcal{W} OR $\mathcal{W}+$ SPACE

In section 4.2, we apply the optimization in the $\mathcal{W}+$ space (denoted as Optim. in $\mathcal{W}+$). Here, we compare this design choice with applying the optimization in the \mathcal{W} space (denoted as Optim. in \mathcal{W}). The quantitative results in Table 8 show that Optim. in $\mathcal{W}+$ achieves lower distortion with a subtle drop in editability. The qualitative results in Figure 14 also show that Optim. in $\mathcal{W}+$ achieves more accurate reconstruction. Thus, we believe that Optim. in $\mathcal{W}+$ is cost-effective compared to the \mathcal{W} space. The reason is that slight

²From <https://twitter.com/robertluxemburg/status/1207087801344372736>

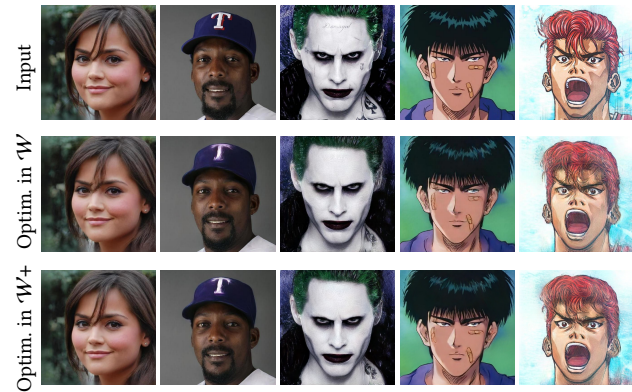


Figure 14: Reconstruction quality comparison. Optim. in $\mathcal{W}+$ means that applying the optimization step in the $\mathcal{W}+$ space.

Table 8: Optim. in $\mathcal{W}+$ means that applying the optimization step in the $\mathcal{W}+$ space. First row: reconstruction evaluation via identity similarity. Second row: editability evaluation via rotation angle.

	PTI [42]	Optim. in \mathcal{W}	Optim. in $\mathcal{W}+$
Identity \uparrow	0.845	0.857	0.866
Angle \uparrow	16.64	22.40	22.20

and local changes (15 iterations in our experiments) to the pivot code can be applied without damaging its editing capability.

E TRAINING METHODOLOGY FOR $\mathcal{W}+\rightarrow\mathcal{W}$

In section 4.1, we propose an training methodology for $\mathcal{W}+\rightarrow\mathcal{W}$ that first gradually increases the weight of the delta regularization loss and then sequentially sets from $\Delta_{N-1} = 0$ to $\Delta_1 = 0$. Increasing the weight of the delta regularization loss can be viewed as a “soft” operation, and setting $\Delta_i = 0$ can be viewed as a “hard” operation. Here, we compare our design choice (denoted as Soft \rightarrow Hard) with sequentially setting from $\Delta_{N-1} = 0$ to $\Delta_1 = 0$ (denoted as Hard). The quantitative results in Table 9 show that our method outperforms the hard operation in both reconstruction and editability. Figure 15 also shows that our method achieves superior editability compared to the hard operation.

F DETAILS OF THE MODELS IN ABLATION STUDY

In section 5.4, we evaluate the proposed cycle encoding by comparing it with three variants: training the encoder in \mathcal{W} , training the encoder in $\mathcal{W}\rightarrow\mathcal{W}+$, and training the encoder in $\mathcal{W}+\rightarrow\mathcal{W}$. Here, we provide the details of the above model configurations. For the first configuration, we train the encoder only in the \mathcal{W} space for 750K iterations using the same hyperparameters as those used in the full approach. For the second configuration, we first train the encoder in the $\mathcal{W}+$ space for 500K iterations and then apply the training methodology described in section 4.1.2 for 250K iterations. For the third configuration, we train the encoder using the training methodology described in section 4.1.1 for 750K iterations.

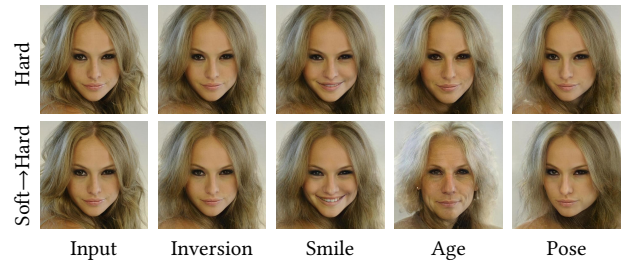


Figure 15: Training methodology for $\mathcal{W}+\rightarrow\mathcal{W}$. Soft \rightarrow Hard denotes the training methodology described in section 4.1.2. Hard denotes the training methodology described in section 4.1.1. The editing is performed using the same editing weight. Soft \rightarrow Hard achieves superior editing quality in terms of editing magnitude.

Table 9: Training methodology for $\mathcal{W}+\rightarrow\mathcal{W}$. First row: reconstruction evaluation via identity similarity. Second row: editability evaluation via rotation angle.

	PTI [42]	Hard	Soft \rightarrow Hard
Identity \uparrow	0.845	0.863	0.866
Angle \uparrow	16.64	11.84	22.20

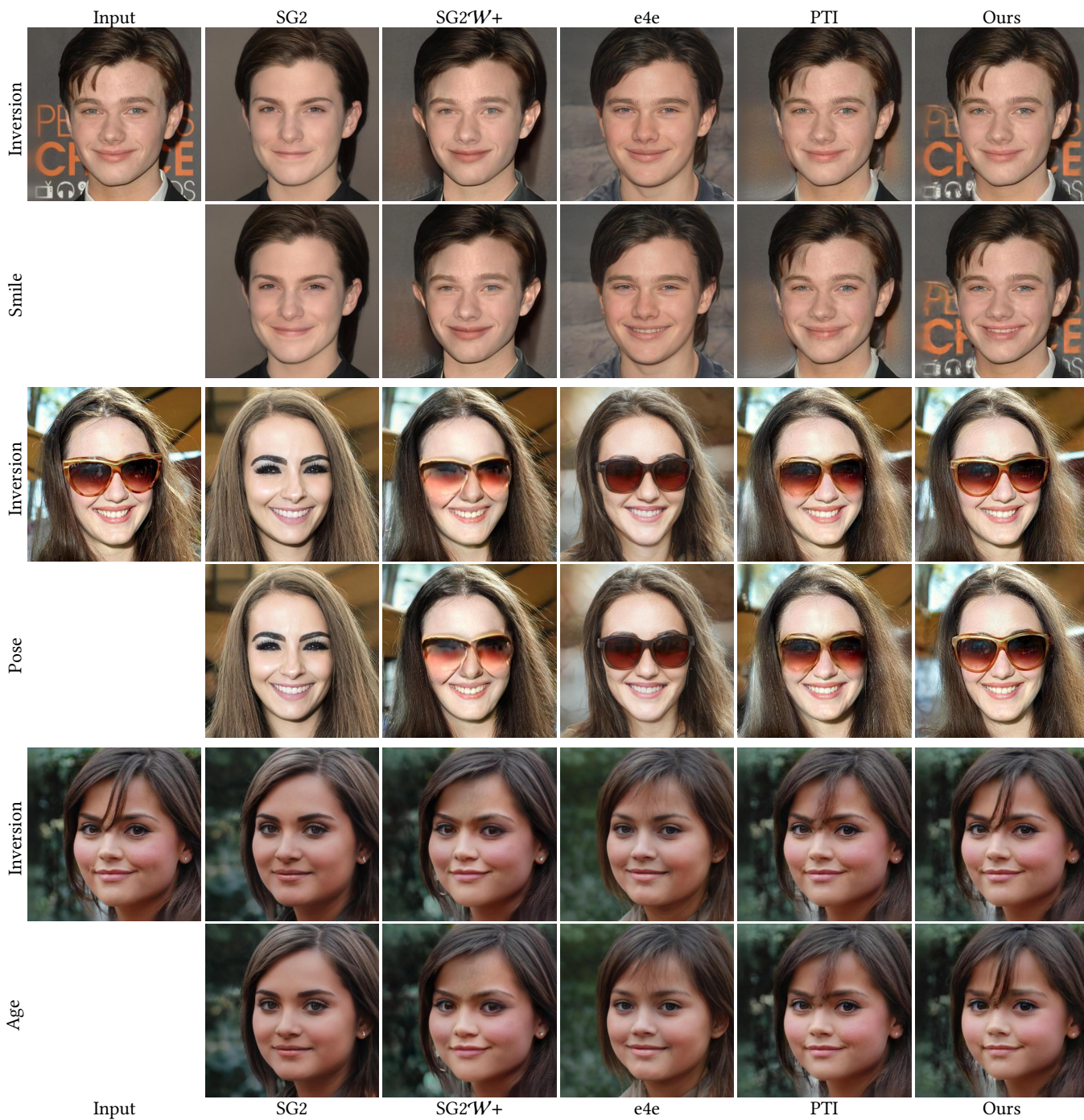


Figure 16: Reconstruction and editing quality comparison using examples from CelebA-HQ test set. In each example, the editing is performed using the same editing weight.

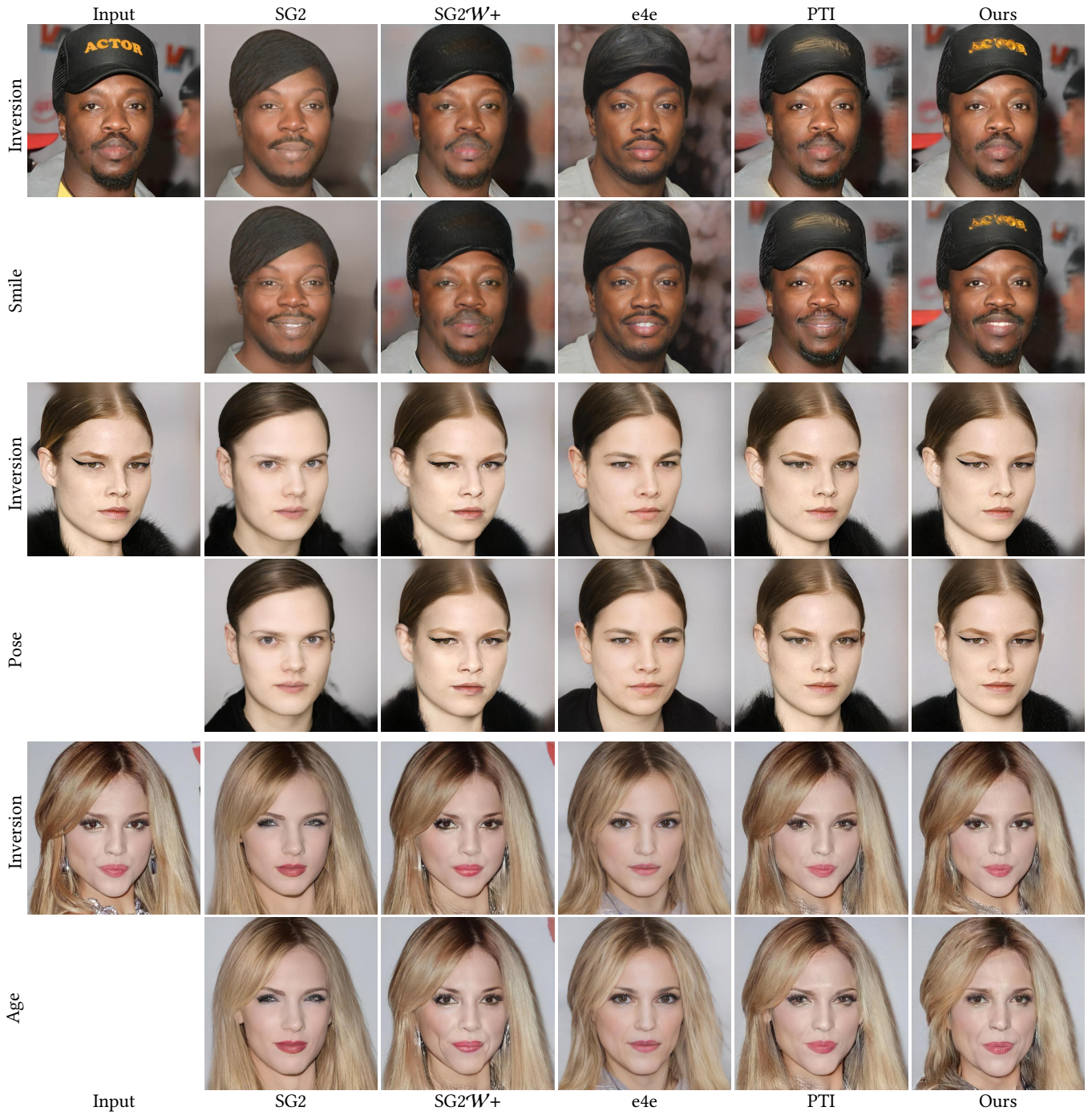


Figure 17: Reconstruction and editing quality comparison using examples from CelebA-HQ test set. In each example, the editing is performed using the same editing weight.

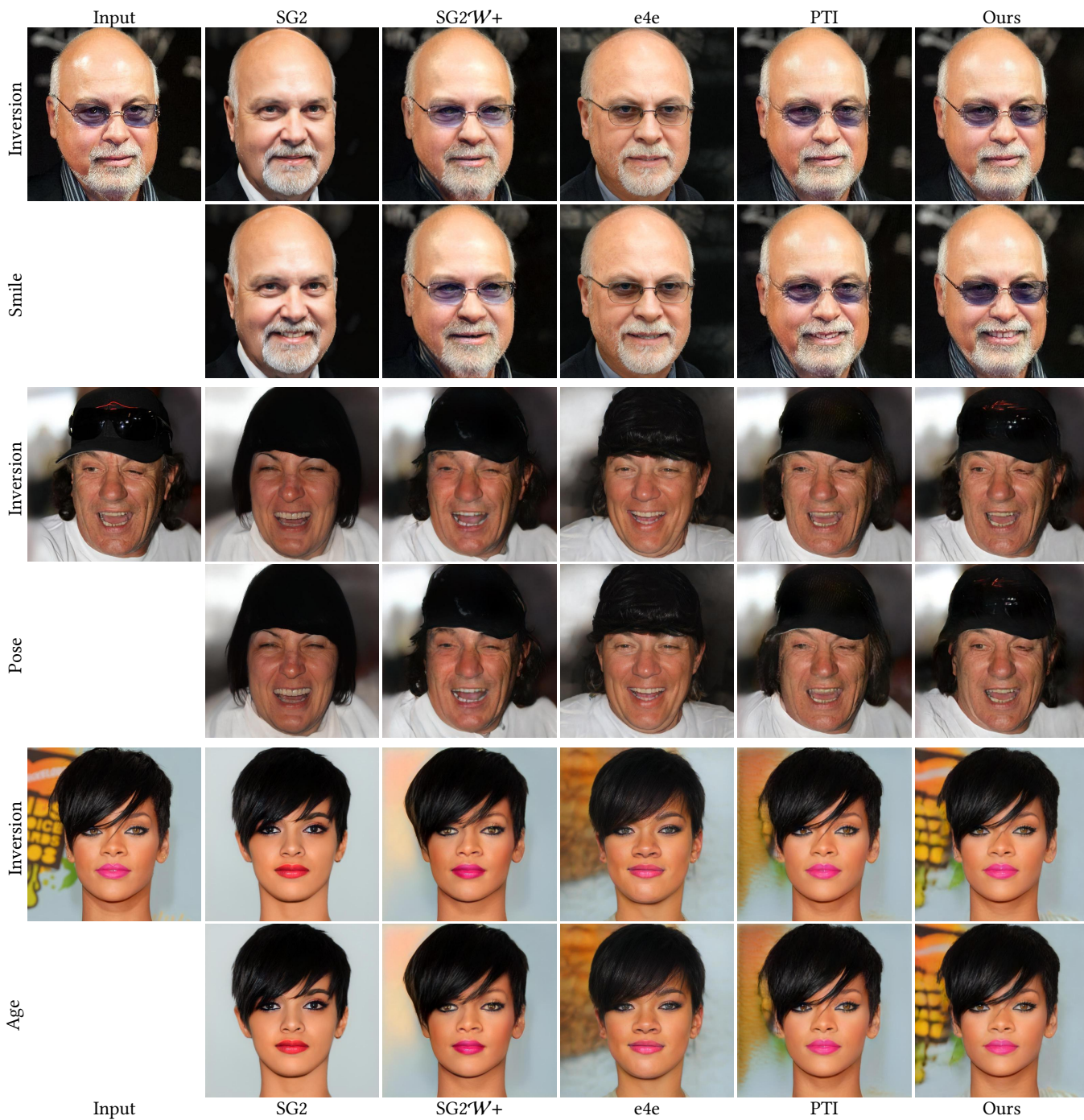


Figure 18: Reconstruction and editing quality comparison using examples from CelebA-HQ test set. In each example, the editing is performed using the same editing weight.



Figure 19: Reconstruction and editing quality comparison using famous character images collected from the web. In each example, the editing is performed using the same editing weight.



Figure 20: Reconstruction and editing quality comparison using famous character images collected from the web. In each example, the editing is performed using the same editing weight.

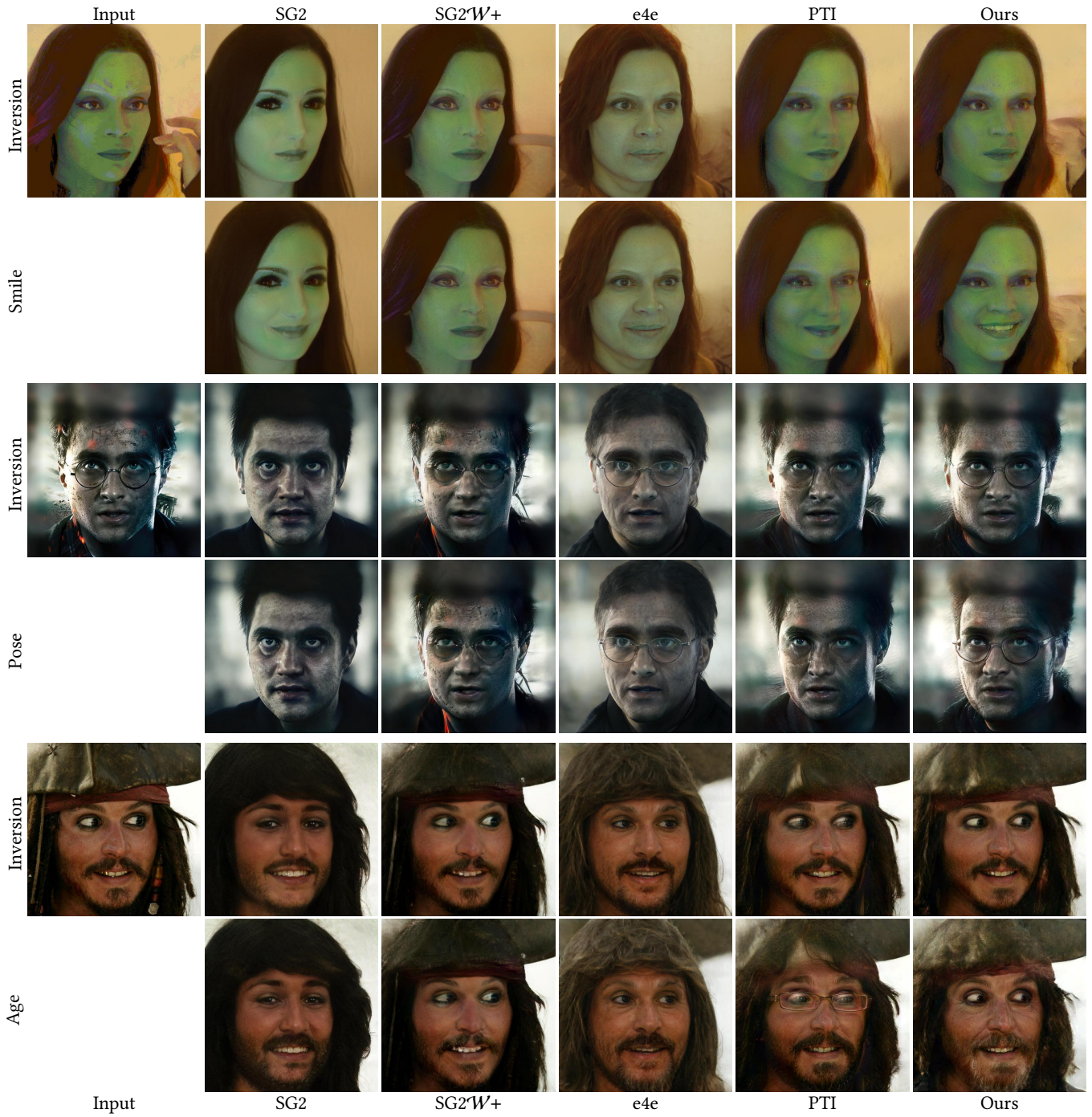


Figure 21: Reconstruction and editing quality comparison using famous character images collected from the web. In each example, the editing is performed using the same editing weight.

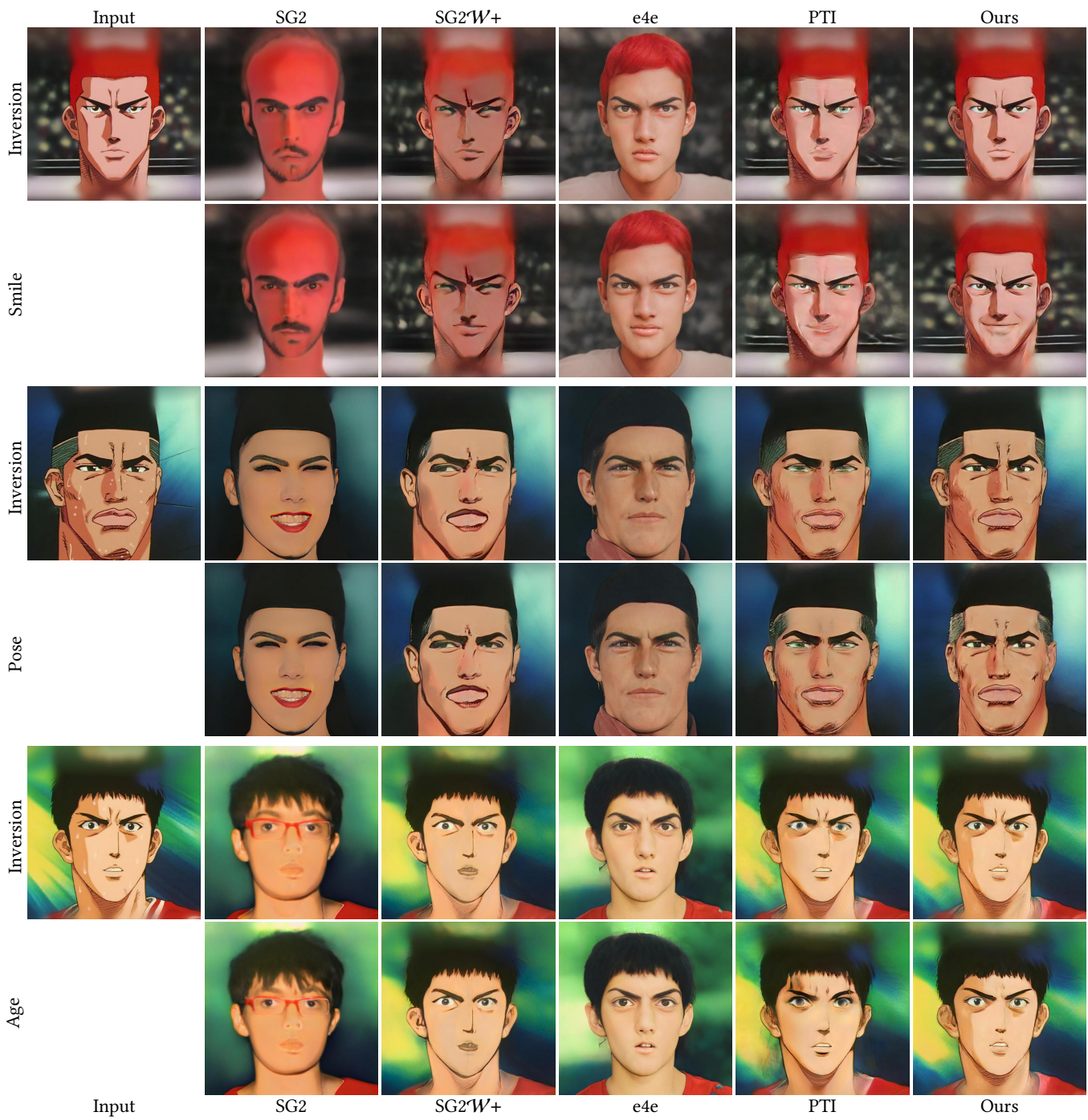


Figure 22: Reconstruction and editing quality comparison using cartoon images collected from the web. In each example, the editing is performed using the same editing weight.

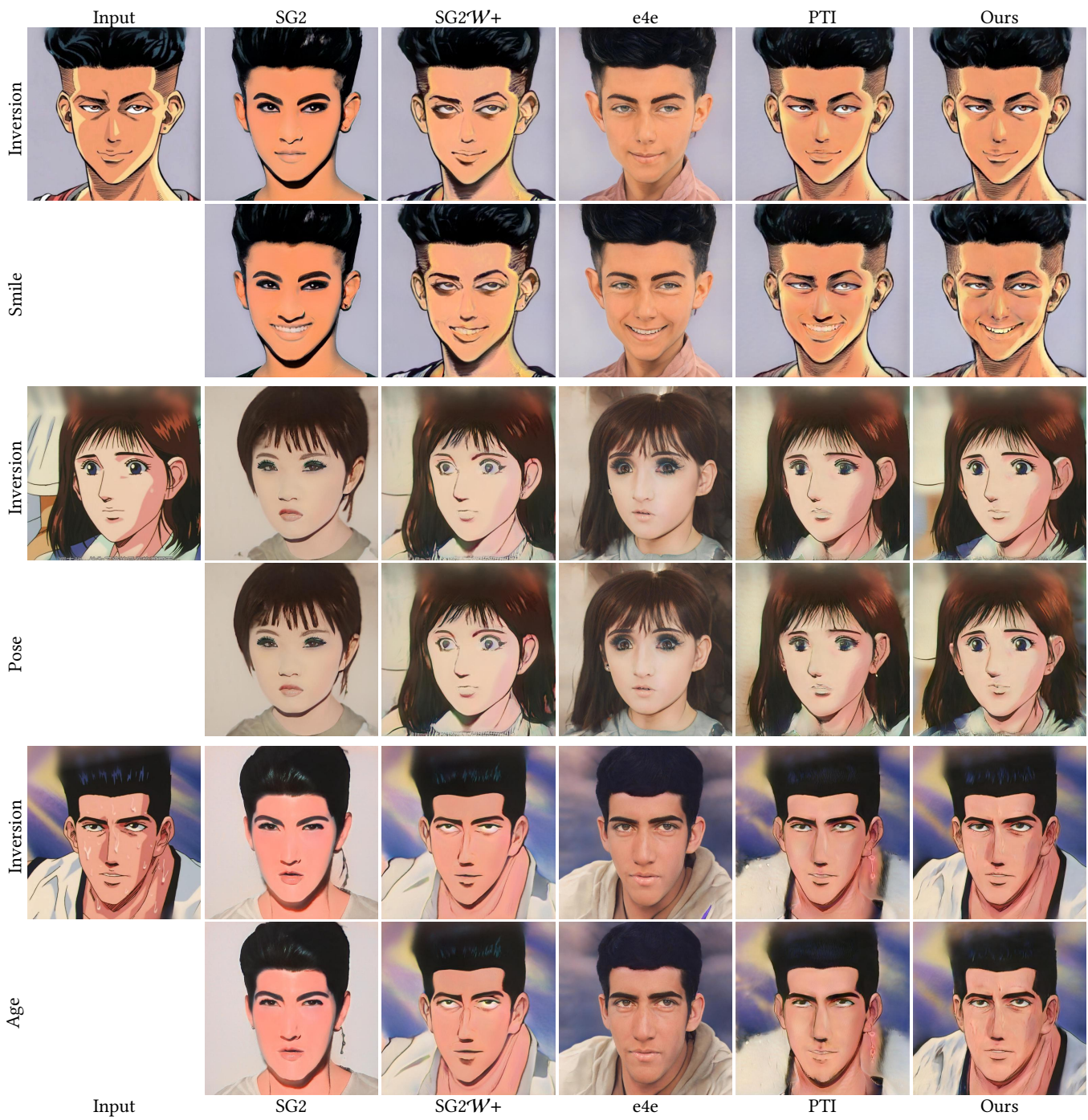


Figure 23: Reconstruction and editing quality comparison using cartoon images collected from the web. In each example, the editing is performed using the same editing weight.

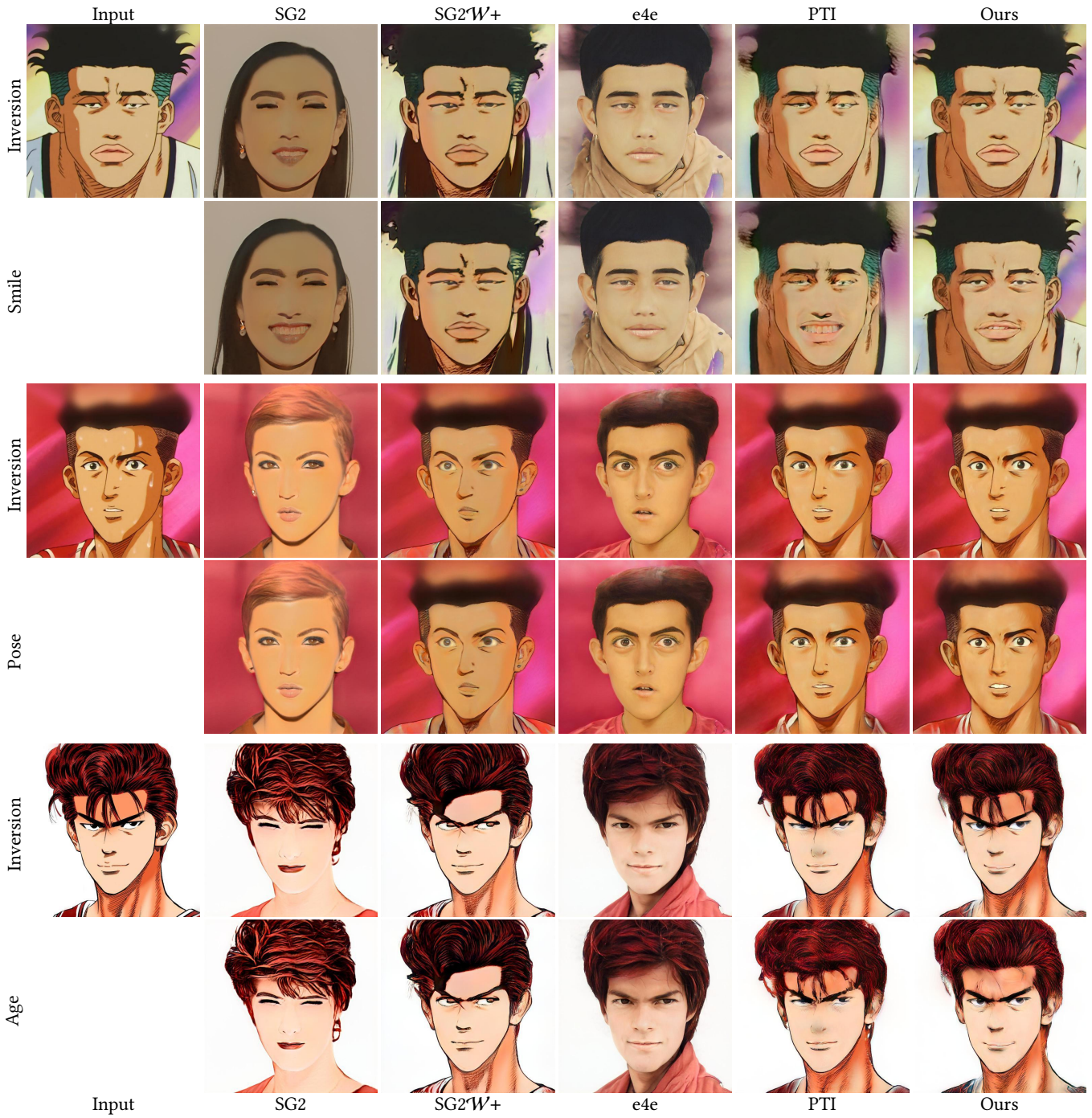


Figure 24: Reconstruction and editing quality comparison using cartoon images collected from the web. In each example, the editing is performed using the same editing weight.

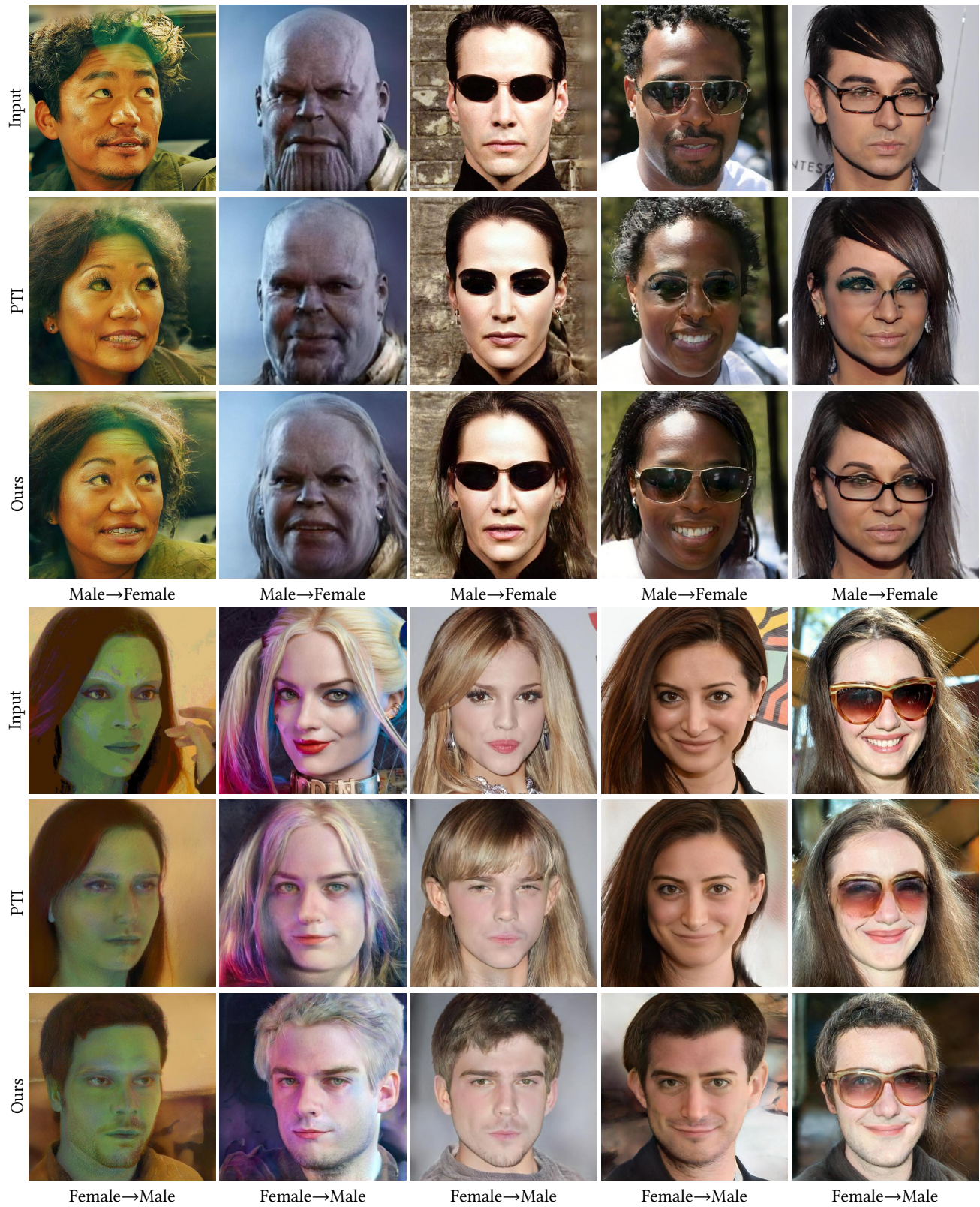


Figure 25: Editing quality comparison using more editing directions. In each example, the editing is performed using the same editing weight.

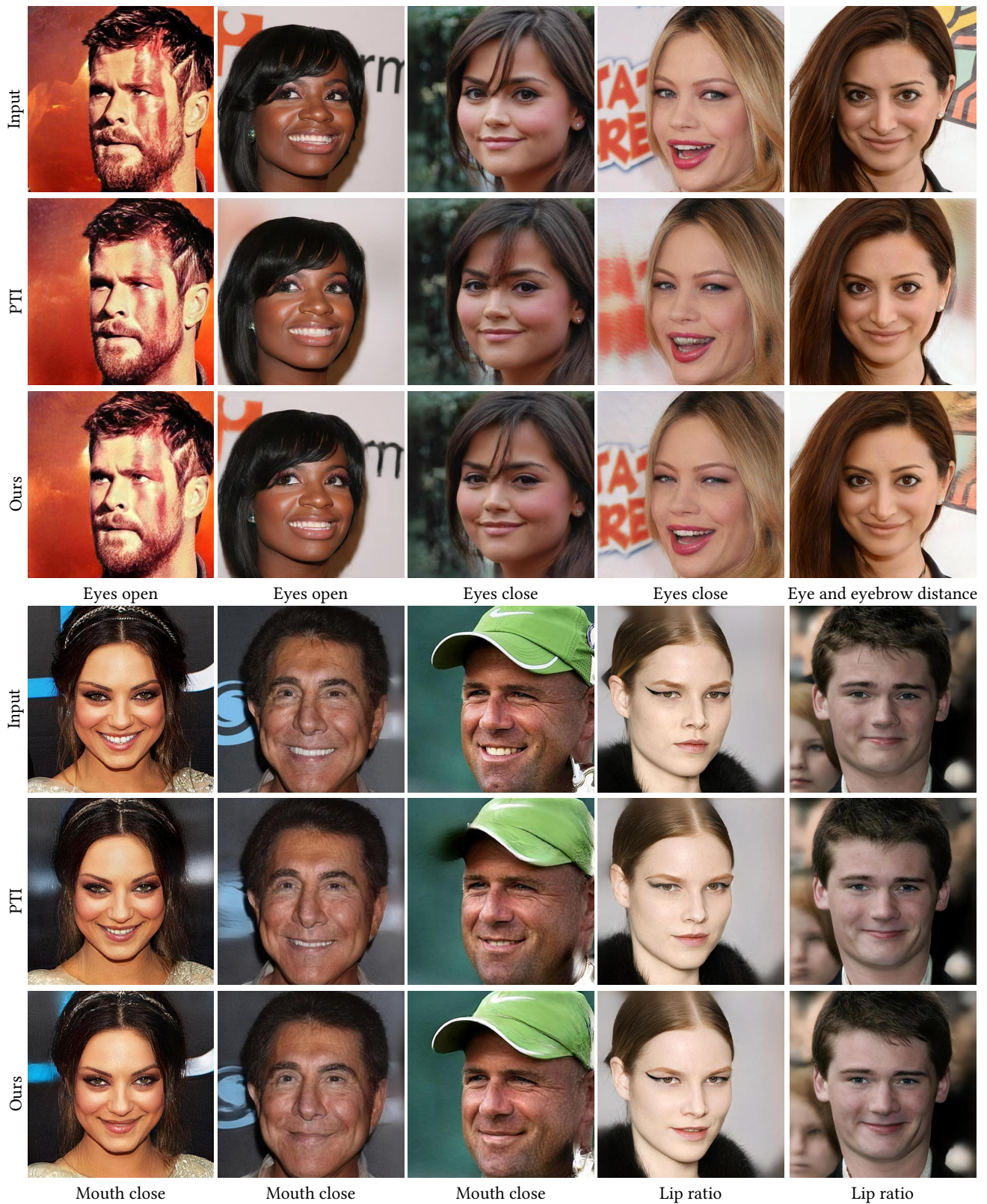


Figure 26: Editing quality comparison using more editing directions. In each example, the editing is performed using the same editing weight.



Figure 27: Afro hairstyle edits using StyleClip [36]. Second row: the original StyleClip model. Third row: PTI uses the optimization-based method for the pivot code. Forth row: PTI uses the e4e model for the pivot code.



Figure 28: Celebrity edits (Mark Zuckerberg) using StyleClip [36]. Second row: the original StyleClip model. Third row: PTI uses the optimization-based method for the pivot code. Forth row: PTI uses the e4e model for the pivot code.